Optical preparation and detection of spin coherence in molecules and crystal defects

Lof, Gerrit

DOI:
10.33612/diss.109567350

Chapter 1

Introduction

1.1 Coherence and polarization of electron spins and photons

For a physical description of the interaction of light and matter, electron spin and polarization of light are of profound importance. Although these concepts have been thoroughly investigated, our understanding of their interaction is far from complete. Common text book examples are e.g. the optical selection rules for the hydrogen atom and GaAs, which are well understood and widely applied for the orientation and probing of spin in these systems. On the other hand, the electronic spin and optical properties of more complex atomic structures such as molecules and crystal defects (with lower symmetry) have not been fully explored. Consequently, modern technology does not fully exploit their potential. The aim of this thesis is to advance the understanding of how optical fields can control and probe electronic spin coherence in molecules and crystal defects.

In 1808, Malus introduced the name polarization for light, while in 1669 already an effect due to light polarization (double refraction) had been reported by Bartholin[1]. The concept of light polarization is used in many applications. Optical communication, however, is mainly based on the detection of light intensity, such that each photon carries at most one bit of information. A polarized photon is said to be in a coherent superposition of polarization states. When information is encoded in the polarization of a photon, each photon can contain a much higher information density, where the practical limitation is set by the ability to discriminate between different polarization states.

In 1925, Uhlenbeck and Goudsmit proposed the concept of spin[2], based on the observation of anisotropic magnetoresistance in 1857[3], and the Stern-

Gerlach experiment in 1922[4]. The most common manifestation of electron spins is in the form of magnetism, for which more and more technological applications are found. Still, within electronic information processing, a bit of information is usually based on the absence or presence of charge. Analogous to polarized photons, spin polarized electrons allow for a larger information density. Also, they are believed to allow for information processing at much lower energy cost. Electron spin polarization occurs when there is a surplus of a certain spin substate, i.e. an imbalance in the (spin-up and spin-down) populations (diagonal elements of the density matrix[5]). For an electron spin brought in a coherent superposition of spin states, the coherences (off-diagonal elements of the density matrix) and spin expectation value oscillate with the so-called Bohr frequencies of the system[5]. Measuring such spin precession instead of merely spin orientation has the experimental advantage that it is much easier to trace back the origin of a small signal when it oscillates. Moreover, one can learn about decoherence and dephasing mechanisms in addition to population relaxation. The electron spin seems very promising to revolutionize electronics[6], particularly through exploiting new (quantum mechanical) concepts like superposition[7] and entanglement[8].

In material systems with selective coupling of photons to electronic spin, they form an attractive pair for opto-electronic functionalities and the transfer of quantum information. This introductory chapter will review different ways to all-optically induce spin coherence (and probe spin dynamics) in various materials, and introduce main concepts that will be used in this thesis. The chapter ends with introducing the specific questions that were addressed in this PhD research, and providing a thesis outline.

1.2 Optical orientation

In many materials, there is naturally an equal amount of both up and down spins. However, in the field of spintronics, which aims to exploit the electron spin, it is important to be able to manipulate the population of spin (or in general total angular momentum) sublevels. More advanced quantum technologies also rely on controlling quantum coherence between spin sublevels. Spin polarization implies an excess of up or down spin, which might e.g. be obtained by applying a strong magnetic field. Alternatively, it can be obtained with a technique called optical orientation (also known as optical spin injection)[9, 10]. Here, an imbalance in the population of spin sublevels is based on different transition strengths for sublevel

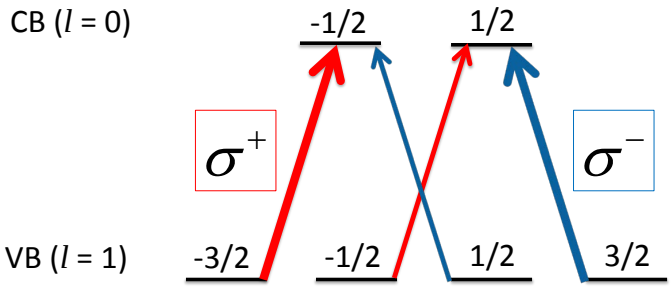

Figure 1.1: Optical selection rules for interband transitions in GaAs for circularly polarized light. The valence band (VB) levels resemble $p_{j=3/2}$ levels of the hydrogen atom, whereas the conduction band (CB) resembles $s_{j=1/2}$ levels. The levels are labeled with m_j-values. The oscillator strengths f of the allowed circular transitions have ratio 1 : 3, where the strong transitions are indicated by thick arrows.

transitions.

Let us as an example consider a direct gap III-V semiconductor like GaAs (with the energy level scheme given in Fig. 1.1). The conduction band (CB) consists of s-like atomic states ($l = 0$), while the valence band (VB) consists of p-like states ($l = 1$). Since electrons and holes have spin $s = 1/2$, the CB consists of a $j = 1/2$ level, while the VB consists of $j = 1/2$ and $j = 3/2$. Due to spin-orbit coupling (SOC) the VB splits, with the $j = 3/2$ level becoming higher in energy.

The VB levels resemble $p_{j=3/2}$ levels of the hydrogen atom, whereas the CB resembles $s_{j=1/2}$ levels. The oscillator strengths f of the allowed circular transitions have ratio 1 : 3, thereby resembling the optical selection rules of hydrogen (Section 2.10, Table 2.5). As illustrated in Fig. 1.1, $\sigma^{\pm}$ light generates three times more electrons with $m_{j=\mp 1/2}$ than with $m_{j=\pm 1/2}$ (when all ground state sublevels are originally equally occupied), thereby inducing spin polarization.

1.3 Spin precession

The Time-Resolved Kerr Readout (TRKR) and Time-Resolved Faraday Rotation (TRFR) technique are techniques (based on the magneto-optical Kerr effect) used to detect spin dynamics and to measure the corresponding lifetime[12, 13]. The difference between TRKR and TRFR is the use of reflected and transmitted light, respectively. These techniques have been applied to many solid state systems like e.g. GaAs. The techniques are optical pump-probe methods with picosecond laser pulses tuned near resonance with transitions across the band gap.

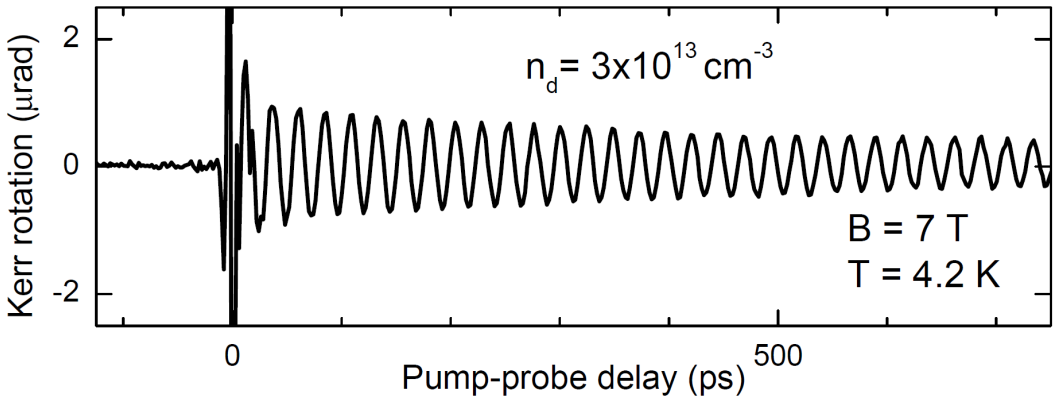

Figure 1.2: Typical result of a Time-Resolved Kerr Rotation (TRKR) experiment, with the Kerr rotation angle as a function of pump-probe delay. The oscillatory character reflects spin precession about the magnetic field. Figure adapted from [11].

Spin polarization is induced with a polarized pump pulse. Let us assume that at time $t = t_{pump}$ the system of Fig. 1.1 is excited with a σ^+ pump pulse propagating along x (with originally the ground state sublevels equally populated), causing population imbalance of the m_j sublevels (in the x-basis) of the excited state, i.e. spin polarization (along the x-axis). With a magnetic field in the z-direction, Larmor spin precession occurs during the interval (t_{pump}, t_{probe}), where the system is in the dark. The spin precesses around the z-axis implying that the expectation value $\langle S_x \rangle (t)$ oscillates. The same holds for $\langle S_y \rangle (t)$, but usually spin precession is measured in one direction only. The precession corresponds to population transfer between the m_j sublevels (in the x-basis).

To detect the spin dynamics, a polarized probe pulse is used. A linearly polarized (denoted as π; here referring to the polarization and not the duration of a pulse) probe pulse propagating in the x-direction arrives at delay time $\Delta t = t_{probe} - t_{pump}$. If the system at time t_{probe} has a net spin polarization, an interesting phenomenon occurs. The unequal filling of the up and down spin sublevels of the conduction band gives rise to a difference in the absorption coefficient for σ^+ and σ^-, resulting in a different refractive index through the Kramers-Kronig relation. Given that π is a superposition of σ^+ and σ^-, a polarization rotation of the linearly polarized probe is induced after interaction with the sample. This rotation angle is called the Kerr or Faraday rotation angle, depending on whether TRKR or TRFR is applied. A typical measurement result of the TRKR technique is depicted in Fig. 1.2, where each data point is obtained from a seperate TRKR measurement[11, 14].

1.4 Coherent population trapping

An alternative way to optically induce spin coherence is via a phenomenon known as coherent population trapping (CPT)[15], which is of great significance in quantum-optical operations that use ground-state spin coherence. This phenomenon occurs when two lasers address a so-called Λ system (with its name derived from the arrows in Fig. 1.3 forming the shape of a Λ) at exact two-photon resonance, i.e. when the two-laser detuning matches the ground-state splitting, as in Fig. 1.3. The ground-state spin system is then driven towards a superposition state that approaches $|\Psi_{CPT}\rangle \propto \Omega_2 |g_1\rangle - \Omega_1 |g_2\rangle$ for ideal spin coherence. Here Ω_n is the Rabi frequency for the driven transition from the $|g_n\rangle$ state to the common excited state. Since the system is now coherently trapped in the ground state, the photoluminescence decreases.

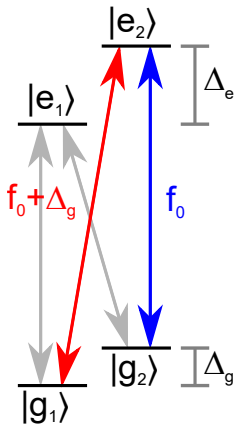

Figure 1.3: Two-laser Λ scheme with optical transitions between $S = 1/2$ ground and excited state sublevels. Two lasers are resonant with transitions from both ground state sublevels $|g_1\rangle$ (red arrow) and $|g_2\rangle$ (blue arrow) to a common excited state sublevel $|e_2\rangle$. This is achieved when the detuning equals the ground-state splitting Δ_g. The gray arrows indicate a secondary Λ scheme via $|e_1\rangle$.

1.5 Jones calculus

To describe how polarized light is affected by interaction with an optical element (or a sample), it is often convenient to use Jones calculus[16] (see also Supplementary Information Section 2.12 (p. 41)). Within this method, light is represented by a Jones vector and the optical element by a Jones matrix. The Jones vector contains the amplitude and phase of the electric field components of the beam

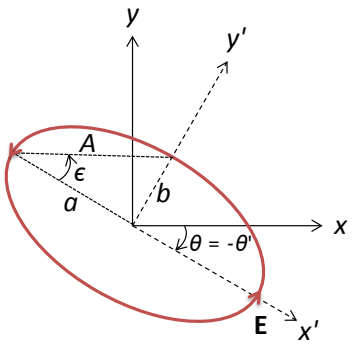

Figure 1.4: The polarization ellipse. The main parameters that define the polarization ellipse are the azimuth θ of the semi-major axis a with respect to the x-axis, and the ellipticity angle ϵ, which is defined through the ellipticity $e = \frac{b}{a}$ (with b the semi-minor axis) such that $e = \pm \tan \epsilon$, where the + and - signs correspond to right- and left-handed polarization respectively. The total amplitude of the electric field is given by $A = \sqrt{a^2 + b^2}$. For convenience, one usually takes $A = 1$. It is also common to assume a global phase factor $\delta = 0$.

orthogonal to its propagation direction. Commonly, the amplitudes are normalized, such that their intensities add up to 1. Any elliptical polarization can be described, including the special cases of linear and circular polarization.

A convenient way to visualize the Jones vector is the polarization ellipse, which is mainly described by the azimuth θ and the ellipticity angle ϵ, as illustrated in Fig. 1.4. Here, the azimuth θ is the angle between the semi-major axis a and the horizontal x-axis, where $-\frac{1}{2}\pi \leqslant \theta \leqslant \frac{1}{2}\pi$. The ellipticity angle ϵ is defined through the ellipticity $e = \frac{b}{a}$ (with b the semi-minor axis) such that $e = \pm \tan \epsilon$, where $-\frac{1}{4}\pi \leqslant \epsilon \leqslant \frac{1}{4}\pi$. The $+$ and $-$ signs correspond to right- and left-handed polarization respectively. In Fig. 1.4 the indicated polarization is left-handed.

Within the $\{\hat{\mathbf{x}}', \hat{\mathbf{y}}'\}$-basis, the corresponding Cartesian Jones vector of a light beam with azimuth $\theta' = 0$ with respect to the x'-axis is given by the unit vector

$$\hat{\mathbf{E}}\{\hat{\mathbf{x}}', \hat{\mathbf{y}}'\} = \begin{bmatrix} \cos(\epsilon) \\ i \sin(\epsilon) \end{bmatrix} \tag{1.1}$$

with amplitude $A = 1$ and global phase $\delta = 0$. This Jones vector can be transformed through a counter-clockwise rotation $\theta' = -\theta$ to

$$\hat{\mathbf{E}}\{\hat{\mathbf{x}}, \hat{\mathbf{y}}\} = T(-\theta) \begin{bmatrix} \cos(\epsilon) \\ i \sin(\epsilon) \end{bmatrix} = \begin{bmatrix} \cos(\theta)\cos(\epsilon) - i \sin(\theta)\sin(\epsilon) \\ \sin(\theta)\cos(\epsilon) + i \cos(\theta)\sin(\epsilon) \end{bmatrix} \tag{1.2}$$

with azimuth $\theta = -\theta'$ (w.r.t the x-axis) and ellipticity angle ϵ. A convenient

method to visualize the Jones vector is via the Poincaré-sphere representation. Within this method, the longitude 2θ and latitude 2ϵ determine a point representing the ellipse of polarization with azimuth θ and ellipticity angle ϵ (Fig. 2.4a).

When light crosses an optical element the resulting polarization of the emerging light is found by taking the product of the Jones matrix J of the optical element and the Jones vector $\mathbf{E}_{in}$ of the incident light, which in the $\{\hat{\mathbf{x}}, \hat{\mathbf{y}}\}$-basis implies

$$\mathbf{E}_{out}\{\hat{\mathbf{x}}, \hat{\mathbf{y}}\} = J\{\hat{\mathbf{x}}, \hat{\mathbf{y}}\}\mathbf{E}_{in}\{\hat{\mathbf{x}}, \hat{\mathbf{y}}\} = J\{\hat{\mathbf{x}}, \hat{\mathbf{y}}\} \begin{bmatrix} E_{in,x} \\ E_{in,y} \end{bmatrix}. \tag{1.3}$$

To build $J\{\hat{\mathbf{x}}, \hat{\mathbf{y}}\}$ we first build $J\{\hat{\mathbf{x}}', \hat{\mathbf{y}}'\}$, which describes how light defined in the $\{\hat{\mathbf{x}}', \hat{\mathbf{y}}'\}$-basis is affected, i.e.

$$\mathbf{E}_{out}\{\hat{\mathbf{x}}', \hat{\mathbf{y}}'\} = J\{\hat{\mathbf{x}}', \hat{\mathbf{y}}'\}\mathbf{E}_{in}\{\hat{\mathbf{x}}', \hat{\mathbf{y}}'\}. \tag{1.4}$$

The Jones matrix is given by

$$J\{\hat{\mathbf{x}}', \hat{\mathbf{y}}'\} = \begin{bmatrix} \mathrm{e}^{i\Lambda n_{x'}} & 0 \\ 0 & \mathrm{e}^{i\Lambda n_{y'}} \end{bmatrix} \tag{1.5}$$

which expresses the retardation of (light polarized along) principal axis $\hat{\mathbf{j}}$ by Λn_j where $\Lambda \equiv 2\pi d/\lambda$, with d the thickness of the sample and λ the wavelength of the light[16].

1.6 Theoretical chemistry methods

The elegance of theoretical chemistry (and physics) calculations and predictions is that properties of matter can be revealed independent of experiments. In this section the theoretical chemistry methods are introduced that are used throughout this work. The methods belong to the realm of quantum chemistry (also known as molecular quantum mechanics), which is a branch of theoretical chemistry aimed to apply quantum mechanics in physical models of chemical systems. As with real experiments, calculations become usually increasingly complicated and expensive with increasing size of the system. To gain better insight into and intuition for chemical and physical properties, it is convenient to first apply theoretical chemistry calculations to a small model system, often allowing for general predictions about more complex matter. For that reason we consider in Chapter 2 the hydrogen atom as a model system. The knowledge obtained here serves as a

theoretical basis for Chapter 3, where several metal-organic molecules are investigated. The main theoretical chemistry method for both chapters is the so-called CASSCF/CASPT2/RASSI–SO method[17, 18], which is an expensive though accurate method for chemical systems to study effects related to spin-orbit coupling (SOC). Additionally, in the Supplementary Information of Chapter 3 also several calculations have been performed based on the density-functional theory (DFT) method, which is one of the most popular quantum chemistry methods due to its versatility and relatively low computational cost.

It is well-known that relativistic effects affect atomic and molecular properties[19–22], particularly when heavy atoms are involved. To account in an accurate way for such effects on excited state properties of molecular systems, the CASSCF/CASPT2/RASSI–SO method was introduced by Roos and Malmqvist[17, 18] (within the quantum chemistry software package MOLCAS[23]). This is a multiconfigurational approach where relativistic effects are treated in two steps, both based on the Douglas–Kroll Hamiltonian[18]. Scalar terms are included in the basis set generation and used to determine wave functions and energies, which include static (through the use of the CASSCF method[24]) and dynamic correlation effects (using multiconfigurational perturbation theory, CASPT2[25, 26]). SOC is added a posteriori by means of the RASSCF state interaction (RASSI[27]) method.

Density functional theory (DFT) is a quantum chemistry method based on the Hohenberg-Kohn (HK) theorem[28], which investigates the electronic structure of many-body systems. Electronic properties can be determined using the spatially dependent electron density functional (i.e. it is a function of another function). The main disadvantage of DFT is the lack of a systematic approach to improve results towards an exact solution[24]. To investigate electronic properties in the presence of time-dependent potentials like electromagnetic waves, time-dependent DFT (TDDFT) is a convenient method, based on the Runge-Gross theorem[29], which is the time-dependent analogue of the HK theorem. In our TDDFT calculations SOC was included perturbatively[30]. For the DFT calculations in this work, we used the Amsterdam Density Functional (ADF) program[31, 32].

1.7 Scope of this research and thesis outline

This thesis focuses on theoretical and experimental studies of optical preparation and detection of spin coherence in molecules and crystal defects. The scientific

progress of this work expands the range of material systems that can have functionalities based on the selective coupling of photons to electronic spin states. Also, it allows for a better opto-electronic characterization of these materials by providing new probing tools. The work consists of a theoretical investigation of underlying fundamentals and forthcoming requirements (Chapter 2-4), and experimental work on a crystal defect in silicon carbide, demonstrating optical characterization of its spin properties and optically induced electron spin coherence (Chapter 5).

Chapter 2 presents a theoretical study of how charged items in the environment of a hydrogen atom perturb its polarization selection rules. We focus on the optical transitions between $1s$ and $2p$ sublevels of the hydrogen atom. We investigate the effect of a gradual distortion of the symmetry by surrounding charges, which provides insight in the gradual evolution of the polarization selection rules. This ability to manipulate optical selection rules allows for better control of the interaction between photons and electrons, which potentially allows for new mechanisms to control the flow of quantum information. Also, this study provides a useful theoretical framework for the more complex systems of later chapters focusing on molecules and crystal defects.

The enormous variety of molecules and their ease of processing make them interesting candidates for many applications. Metal-organic molecules can have large spin-orbit coupling (SOC), which may facilitate mechanisms for optical spin manipulation. The Time-Resolved Faraday Rotation technique (TRFR, already widely applied to conventional semiconductors) is here of interest, since it is an all-optical technique that can induce and probe the quantum dynamics of spin with ultra-fast time resolution. However, whether (and how) TRFR can be applied to study spin dynamics of triplet (spin $S = 1$) states in molecules was an open question. We explore in **Chapter 3** how TRFR can be applied to molecules with strong SOC, exploiting the optical selection rules for transitions between singlet and triplet states in such molecules. We define how one can study polarization and quantum dynamics of spin after excitation to a superposition of triplet sublevels, using an ultrashort pump pulse. We use the polarization rotation of an ultrashort probe pulse as a measure for the coherent spin dynamics. Besides using this in fundamental studies of the spin properties of such molecules, these results are of value for advancing opto-electronic and spintronic applications.

Until now, all cases where the TRFR technique was used for studying coherent spin dynamics concerned materials systems with strong SOC. Strong SOC may seem a requirement, since it facilitates optical selection rules with allowed

transitions that alter the spin state (otherwise only spin-conserving transitions seem allowed). However, **Chapter 4** defines how the TRFR technique can also be applied to certain material systems with negligible SOC. In our derivations we focus on the characterization of spin-active color centers in materials like silicon carbide and diamond. Such color centers are recognized as promising systems for quantum technologies since they can combine long-coherent electronic spin and bright optical properties. We introduce the theory of a TRFR experiment applied to divacancies in silicon carbide, based on non-spin-conserving optical selection rules that can emerge due to the anisotropic spin $S = 1$ Hamiltonian for the electronic ground and excited state of this system.

Finally, **Chapter 5** presents an experimental investigation of the molybdenum-impurity in silicon carbide. We demonstrate an all-optical technique for characterizing the spin Hamiltonians for the ground and excited state, and find that these are $S = 1/2$ systems with highly anisotropic spin properties. In turn, we exploit these properties for tuning control schemes where two-laser driving addresses transitions of a Λ system, and observe coherent population trapping for the ground-state spin. These results demonstrate that the Mo defect and similar transition-metal impurities in silicon carbide may be relevant for advancing quantum communication and quantum sensing technology. In particular, these systems have optical transitions at near-infrared wavelengths (in or close to telecom communication bands), and the device technology for silicon carbide is already available at a high level in industry.

Supplementary Information (SI)

1.8 SI: Change of basis

A choice of a basis is not unique. Let us perform a change of orthonormal bases, from the (old) basis $\{\hat{\mathbf{x}}', \hat{\mathbf{y}}'\}$ to the (new) basis $\{\hat{\mathbf{x}}, \hat{\mathbf{y}}\}$, through a counter-clockwise rotation with angle θ', as depicted in Fig. 1.5. Consider the vector $\mathbf{E}$ (which e.g. can be considered as the electric field component of a light beam),

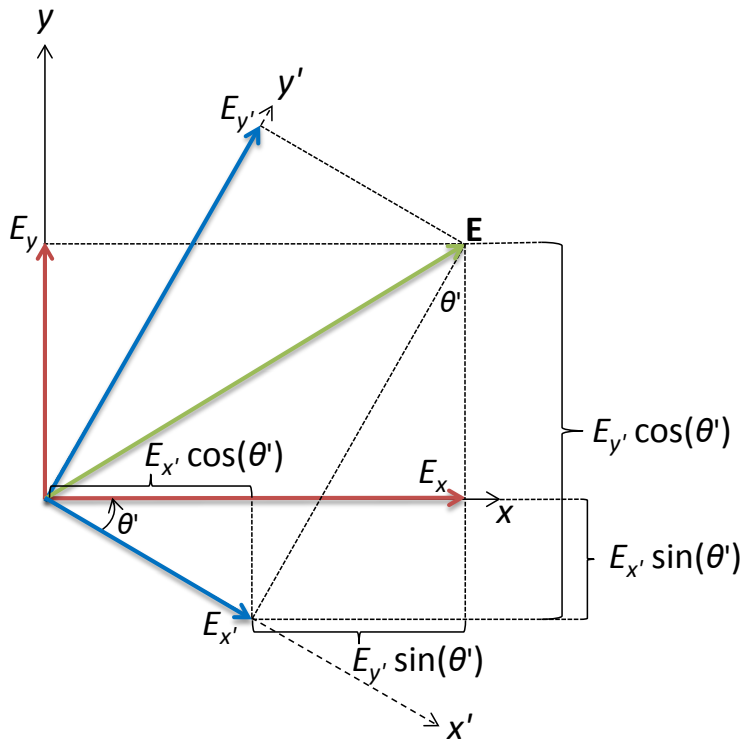

Figure 1.5: Illustration of a change of orthonormal bases. The transformation is from the (old) basis $\{\hat{\mathbf{x}}', \hat{\mathbf{y}}'\}$ to the (new) basis $\{\hat{\mathbf{x}}, \hat{\mathbf{y}}\}$, through a counter-clockwise rotation with angle θ'. To derive the transformation matrix $T_{\{\hat{\mathbf{x}}', \hat{\mathbf{y}}'\} \to \{\hat{\mathbf{x}}, \hat{\mathbf{y}}\}}$, the change of basis is applied to the vector $\mathbf{E}$, which e.g. can be considered as the electric field component of a light beam.

which in the old basis is given by

$$\mathbf{E}\{\hat{\mathbf{x}}', \hat{\mathbf{y}}'\} = E_{x'}\hat{\mathbf{x}}' + E_{y'}\hat{\mathbf{y}}' = \begin{bmatrix} E_{x'} \\ E_{y'} \end{bmatrix} \tag{1.6}$$

In the new basis, we have instead

$$\mathbf{E}\{\hat{\mathbf{x}}, \hat{\mathbf{y}}\} = E_x\hat{\mathbf{x}} + E_y\hat{\mathbf{y}} = \begin{bmatrix} E_{x'}\cos(\theta') + E_{y'}\sin(\theta') \\ E_{y'}\cos(\theta') - E_{x'}\sin(\theta') \end{bmatrix} \tag{1.7}$$

The vector $\mathbf{E}$ can be easily transformed from the old basis to the new one through the matrix transformation

$$\mathbf{E}\{\hat{\mathbf{x}}, \hat{\mathbf{y}}\} = T_{\{\hat{\mathbf{x}}', \hat{\mathbf{y}}'\} \to \{\hat{\mathbf{x}}, \hat{\mathbf{y}}\}} \mathbf{E}\{\hat{\mathbf{x}}', \hat{\mathbf{y}}'\} \tag{1.8}$$

which corresponds to

$$\begin{bmatrix} E_x \\ E_y \end{bmatrix} = \begin{bmatrix} \cos(\theta') & \sin(\theta') \\ -\sin(\theta') & \cos(\theta') \end{bmatrix} \begin{bmatrix} E_{x'} \\ E_{y'} \end{bmatrix} \tag{1.9}$$

where the transformation matrix $T(\theta')$ has as its columns the old unit vectors as written in the new basis, i.e.

$$\hat{\mathbf{x}}'\{\hat{\mathbf{x}}, \hat{\mathbf{y}}\} = x'_x\hat{\mathbf{x}} + x'_y\hat{\mathbf{y}} = \begin{bmatrix} x'_x \\ x'_y \end{bmatrix} = \begin{bmatrix} \cos(\theta') \\ -\sin(\theta') \end{bmatrix} \tag{1.10}$$

$$\hat{\mathbf{y}}'\{\hat{\mathbf{x}}, \hat{\mathbf{y}}\} = y'_x\hat{\mathbf{x}} + y'_y\hat{\mathbf{y}} = \begin{bmatrix} y'_x \\ y'_y \end{bmatrix} = \begin{bmatrix} \sin(\theta') \\ \cos(\theta') \end{bmatrix} \tag{1.11}$$

where e.g. x'_x denotes the x-component of $\hat{\mathbf{x}}'$, i.e. the projection of $\hat{\mathbf{x}}'$ onto $\hat{\mathbf{x}}$.

Any matrix M defined in the old basis can be described by the new basis through the following unitary similarity transformation

$$M\{\hat{\mathbf{x}}, \hat{\mathbf{y}}\} = T_{\{\hat{\mathbf{x}}', \hat{\mathbf{y}}'\} \to \{\hat{\mathbf{x}}, \hat{\mathbf{y}}\}} M\{\hat{\mathbf{x}}', \hat{\mathbf{y}}'\} T^{\dagger} \tag{1.12}$$

with $T^{\dagger}$ the Hermitian adjoint (conjugate transpose) of T, which has the properties $T^{\dagger}(\theta') = T^{-1}(\theta') = T(-\theta')$, and it has the unit vectors $\hat{\mathbf{x}}\{\hat{\mathbf{x}}', \hat{\mathbf{y}}'\}$ and $\hat{\mathbf{y}}\{\hat{\mathbf{x}}', \hat{\mathbf{y}}'\}$ as its columns, i.e.

$$\hat{\mathbf{x}}\{\hat{\mathbf{x}}', \hat{\mathbf{y}}'\} = x_{x'}\hat{\mathbf{x}}' + x_{y'}\hat{\mathbf{y}}' = \begin{bmatrix} x_{x'} \\ x_{y'} \end{bmatrix} = \begin{bmatrix} \cos(\theta') \\ \sin(\theta') \end{bmatrix} \tag{1.13}$$

$$\hat{\mathbf{y}}\{\hat{\mathbf{x}}', \hat{\mathbf{y}}'\} = y_{x'}\hat{\mathbf{x}}' + y_{y'}\hat{\mathbf{y}}' = \begin{bmatrix} y_{x'} \\ y_{y'} \end{bmatrix} = \begin{bmatrix} -\sin(\theta') \\ \cos(\theta') \end{bmatrix} \tag{1.14}$$

1.9 SI: Jones calculus applied to a waveplate

To get familiar with Jones calculus, we take here waveplates as an example. We will show that an optical element can be described by a Jones matrix, which transforms the electric vector of an incoming beam via a matrix multiplication. We also illustrate the transformation of one coordinate system to another via a matrix transformation.

Usually, a waveplate has real-valued principal axes (often denoted as $|H\rangle$ and $|V\rangle$), which we denote as $\hat{\mathbf{x}}'$ and $\hat{\mathbf{y}}'$. Consequently, the corresponding Jones matrix is diagonal in the $\{\hat{\mathbf{x}}', \hat{\mathbf{y}}'\}$-basis, and given by Eq. (1.5).

Let us consider two special cases of the waveplate, namely the half-waveplate (HWP) and the quarter-waveplate (QWP). A HWP has its thickness such that the phase difference between the components is given by $\Lambda n_{y'} - \Lambda n_{x'} = \pi$. Also, only the vertical component $\hat{\mathbf{y}}'$ (slow axis) gets retarded by the HWP, whereas the horizontal component $\hat{\mathbf{x}}'$ (fast axis) is not affected, such that the Jones matrix is given by

$$J_{HWP}\{\hat{\mathbf{x}}', \hat{\mathbf{y}}'\} = \begin{bmatrix} 1 & 0 \\ 0 & -1 \end{bmatrix} \tag{1.15}$$

The effect of a HWP on an incident linearly polarized beam is that its azimuth (w.r.t. the fast axis x') gets reflected in the fast axis, as illustrated in Fig. 1.6. This follows from substituting Eq. (1.15) into Eq. (1.4) and taking real-valued $E_{x'}$ and $E_{y'}$, which yields $E_{y'} \to -E_{y'}$, i.e. $\theta' \to -\theta'$. Alternatively, one could apply Eq. (1.3), which requires the transformation $J\{\hat{\mathbf{x}}', \hat{\mathbf{y}}'\} \to J\{\hat{\mathbf{x}}, \hat{\mathbf{y}}\}$ via Eq. (1.12). For a HWP with its fast axis at angle $\theta = -\theta'$ (w.r.t. the x-axis) this requires a counter-clockwise rotation with angle θ' (w.r.t. the x'-axis), which gives according to Eq. (1.12)

$$\begin{aligned} J_{HWP}\{\hat{\mathbf{x}}, \hat{\mathbf{y}}\} &= \begin{bmatrix} \cos(\theta') & \sin(\theta') \\ -\sin(\theta') & \cos(\theta') \end{bmatrix} \begin{bmatrix} 1 & 0 \\ 0 & -1 \end{bmatrix} \begin{bmatrix} \cos(\theta') & -\sin(\theta') \\ \sin(\theta') & \cos(\theta') \end{bmatrix} \\ &= \begin{bmatrix} \cos(2\theta') & -\sin(2\theta') \\ -\sin(2\theta') & -\cos(2\theta') \end{bmatrix} \end{aligned} \tag{1.16}$$

Substituting into Eq. (1.3) gives for an incident beam with Jones vector $\hat{\mathbf{E}}_{in} = \hat{\mathbf{x}}$

$$\hat{\mathbf{E}}_{out}\{\hat{\mathbf{x}}, \hat{\mathbf{y}}\} = \begin{bmatrix} \cos(2\theta') & -\sin(2\theta') \\ -\sin(2\theta') & -\cos(2\theta') \end{bmatrix} \begin{bmatrix} 1 \\ 0 \end{bmatrix} = \begin{bmatrix} \cos(2\theta') \\ -\sin(2\theta') \end{bmatrix} \tag{1.17}$$

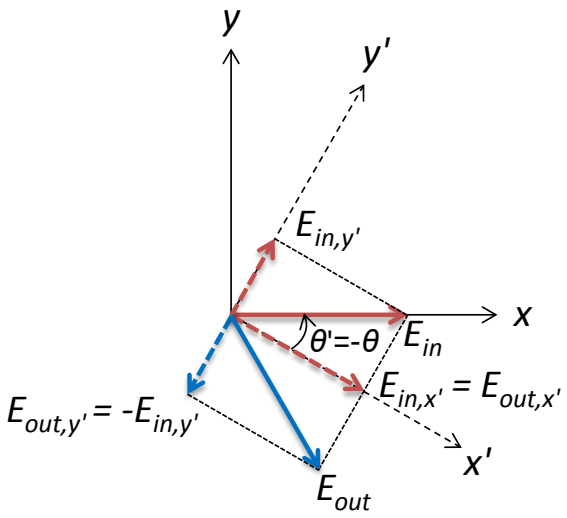

Figure 1.6: The effect of a half-waveplate (HWP) on an incident linearly polarized beam. For a beam polarized along $\hat{\mathbf{x}}$, the azimuth θ' (w.r.t. the fast axis $\hat{\mathbf{x}}'$) gets reflected in the fast axis.

which corresponds to an azimuth of $\theta = -2\theta'$ (w.r.t. the x-axis), as it should.

A QWP has its thickness such that the phase difference between the components is given by $\Lambda n_{y'} - \Lambda n_{x'} = \pi/2$. Also, only the vertical component (slow axis) gets retarded by the QWP, whereas the horizontal component (fast axis) is not affected, such that the Jones matrix is given by

$$J_{QWP}\{\hat{\mathbf{x}}', \hat{\mathbf{y}}'\} = \begin{bmatrix} 1 & 0 \\ 0 & i \end{bmatrix} \tag{1.18}$$

which e.g. makes a linear beam with azimuth $\theta' = 45°$ (w.r.t. the fast x'-axis) circularly polarized. For a QWP with its fast axis at angle $\theta = -\theta'$ w.r.t. the x-axis (i.e. the x-axis is at θ' w.r.t. the x'-axis), one obtains in analogy to Eq. (1.16)

$$J_{QWP}\{\hat{\mathbf{x}}, \hat{\mathbf{y}}\} = \begin{bmatrix} \cos^2(\theta') + i\sin^2(\theta') & (-1+i)\sin(\theta')\cos(\theta') \\ (-1+i)\sin(\theta')\cos(\theta') & \sin^2(\theta') + i\cos^2(\theta') \end{bmatrix} \tag{1.19}$$